

## Multi-field Coupling of Particulate Systems

K. Han<sup>1</sup>, Y. T. Feng<sup>1</sup> and D. R. J. Owen<sup>1</sup>

**Abstract:** A computational framework is established for effective modelling of fluid-thermal-particle interactions. The numerical procedures comprise the Discrete Element Method for simulating particle dynamics; the Lattice Boltzmann Method for modelling the mass and velocity field of the fluid flow; and the Discrete Thermal Element Method and the Thermal Lattice Boltzmann Method for solving the temperature field. The coupling of the three fields is realised through hydrodynamic interaction force terms. Selected numerical examples are provided to illustrate the applicability of the proposed approach.

**Keywords:** multi-field coupling, particulate systems, Discrete Element Method, Lattice Boltzmann Method, Discrete Thermal Element Method, transient analysis.

### 1 Introduction

In recent years the modelling of coupled field problems, in which two or more physical fields contribute to the system response, has become a focus of major research activity. Among them, the quantitative study of fluid-thermal-particle interaction problems encountered in many engineering applications is of fundamental importance. For instance, the mineral recovery operation in the mining industry employs a suction process to extract rock fragments from the ocean or river bed. The computational modelling of this particle transport problem requires a fluid-particle interaction simulation. The motion of the particles is driven collectively by the gravity and the hydrodynamic forces exerted by the fluid, and may also be altered by the interaction between the particles. On the other hand, the fluid flow pattern can be greatly affected by the presence of the particles, and is often of a turbulent nature. In the nuclear industry, the process of a pebble bed nuclear reactor essentially involves the forced flow of gas through uranium enriched spheres that are cyclically fed through a concentric column in order to extract thermal energy. In this situation, the introduction of additional field, thermal (heat transfer between

---

<sup>1</sup> Civil and Computational Engineering Centre, School of Engineering, Swansea University, SA2 8PP, UK

the moving particles in the form of conduction, convection, and radiation, as well as transfer of heat to the gas stream), poses even more computational challenges.

The fundamental physical phenomena involved in these systems are generally not well understood and often described in an empirical fashion, mainly due to the intricate complexity of the hydrodynamic and thermodynamic interactions exhibited and the non-existence of high-fidelity modelling capability.

Although the Finite Element Method has a powerful capability of modelling the nonlinear response of continua, and significant progress has also been made in the modelling of contact of deformable bodies, the continuum nature of its algorithmic framework imposes restrictions when dealing with discontinuous media. Firstly, it is not efficient with the finite element representation of a large number of discrete objects whose deformation is of secondary importance. Secondly, the contact detection procedures available in the Finite Element Method are not adequate to handle contact with constantly changing and evolving configurations in an unpredictable manner. Consequently an alternative numerical approach within a discontinuous framework has been exploited. The Discrete Element Method, among other discontinuous methodologies such as Discontinuous Deformation Analysis and the Manifold Method, has become a promising numerical tool capable of simulating problems of a discrete or discontinuous nature. In the framework of the Discrete Element Method, a discrete system is considered as an assembly of individual discrete objects which are treated as rigid and represented by discrete elements as simple geometric entities. The dynamic response of discrete elements depends on the interaction forces which can be short-ranged, such as mechanical contact, and/or medium-ranged, such as attraction forces in liquid bridges, and obey Newton's second law of motion. By tracking the motion of individual discrete elements and handling their interactions, the dynamic behaviour of a discrete system can be simulated.

Conventional computational fluid dynamic methods have limited success in simulating particulate flows with a high number of particles due to the need to generate new, geometrically adapted grids, which is a very time-consuming task especially in three-dimensional situations (Feng *et al* 2004). In contrast, the Lattice Boltzmann Method (LBM) overcomes the limitations of the conventional numerical methods by using a fixed, non-adaptive (Eulerian) grid system to represent the flow field. In particular, it can efficiently model fluid flows in complex geometries, as is the case of particulate flow under consideration. A rich publication in recent years (see for instance, Aidun *et al* 1998, Cook *et al* 2004, Feng *et al* 2007, Feng *et al* 2009, Feng *et al* 2004, Han *et al* 2007a, Ho *et al* 2009, Ladd 1994, Ladd *et al* 2001, Mishra *et al* 2009, Qi *et al* 2003, and the references therein) has proved the effectiveness of the method.

In our previous studies (Feng *et al* 2007, Feng *et al* 2009, Han *et al* 2007a), the Lattice Boltzmann Method and the Discrete Element Method have been successfully coupled for the simulation of fluid-particle interaction problems, where the fluid field is solved by the extended lattice Boltzmann equation with the incorporation of the Smagorinsky turbulence model, while the particle dynamics is simulated by the Discrete Element Method. The hydrodynamic interactions between the fluid and particles are realised through an immersed boundary condition.

If an additional field, thermal, is introduced to a particulate system, the Thermal Lattice Boltzmann Method may be employed to model heat transfer between particles and between particles and the surrounding fluid. Our numerical tests show, however, that the Thermal Lattice Boltzmann Method is not efficient for simulating heat conduction in particles. For this reason, a novel numerical scheme, termed the Discrete Thermal Element Method (Feng *et al* 2008), is put forward. In this approach, each particle is treated as an individual element with the number of (temperature) unknowns equal to the number of particles that it is in contact with. The element thermal conductivity matrix can be very effectively evaluated and is entirely dependent on the contact characteristics. This new element shares the same form and properties with its conventional thermal finite element counterpart. In particular, the entire solution procedure can follow exactly the same steps as those involved in the finite element analysis. Unlike finite elements or other numerical techniques, no discretisation errors are involved in the Discrete Thermal Element Method. The numerical validation against the finite element solution indicates that the solution accuracy of this scheme is reasonable and highly efficient in particular.

The fluid-thermal-particle interaction problems is often of a dynamic and transient nature. Although the Discrete Thermal Element Method is capable of modelling the steady-state heat conduction in large particulate systems efficiently, it is not trivial to be extended to transient situations. Meanwhile, its formulation is not compatible with that of the Discrete Element Method which accounts for particle-particle interactions. Therefore the Discrete Thermal Element Method needs to be modified to realise thermal-particle coupling. The pipe-network model is such a modification, in which each particle is replaced by a thermal pipe-network connecting the particle's centre with each contact zone associated with the particle.

The objective of this work is to present essential computational procedures for the effective coupling of fluid-thermal-particle interaction problems. In what follows, the basic formulations of the Discrete Element Method, the Lattice Boltzmann Method, the Discrete Thermal Element Method, and the coupling techniques, will be outlined. Selected numerical examples are provided to illustrate the applicability of the proposed approach.

## 2 Particle-Particle Interactions

Interactions between the moving particles are modelled by the Discrete Element Method, in which each discrete object is treated as a geometrically simplified entity that interacts with other discrete objects through boundary contact. At each time step, objects in contact are identified with a contact detection algorithm; and the contact forces are evaluated based on appropriate interaction laws. The motion of each discrete object is governed by Newton's second law of motion. A set of governing equations is built up and integrated with respect to time, to update each object's position, velocity and acceleration. The main building blocks of the discrete element procedure are described as follows.

### 2.1 Representation of discrete objects

In the Discrete Element Method, discrete objects are treated as rigid and represented either by regular geometric shapes, such as disks, spheres and superquadrics, or by irregular geometric shapes, such as polygons, polyhedrons, clustering or clumping of regular shapes to form compound shapes.

Circular and spherical elements are the most used discrete elements due to their geometric simplicity, smooth and continuous boundary. Contact resolution for this type of element is therefore trivial and computationally efficient. However, idealising materials such as grains and concrete aggregates as perfect disks (or spheres) is not always realistic and may not produce correct dynamic behaviour. One of the reasons is that circular and spherical elements cannot provide resistance to rolling motion. This has led to the introduction of more sophisticated elements to represent the discrete system more realistically.

Contrary to the circular and spherical elements where only the radius can be modified, polygonal elements (polygons or polyhedrons) offer increased flexibility in terms of shape variation. Since the boundary of this type of element is not smooth, some complex situations such as corner/corner contact, often arise in the contact resolution.

Higher order discrete elements can be used, such as superquadrics and hyperquadrics as proposed in (William *et al* 1995), which may represent many simple geometric entities (for instance, disk, sphere, ellipse and ellipsoid) within the framework. However, this mathematical elegance may be offset by the expensive computation involved in the contact resolution.

### 2.2 Contact detection

In the discrete element simulation of problems involving a large number of discrete objects, as much as 60-70% of the computational time could be spent in detecting

and tracking the contact between discrete objects. Due to a large diversity of object shapes, many efficient contact processing algorithms often adopt a two-phase solution strategy. The first phase, termed contact detection or global search, identifies the discrete objects which are considered as potential contactors of a given object. The second phase, termed contact resolution or local search, resolves the details of the contact pairs based on their actual geometric shapes.

Some search algorithms used in general computing technology and computer graphics have been adopted for this purpose. Algorithms such as bucket sorting, heap sorting, quick sorting, binary tree and quadrant tree data structure all originated from general computing algorithms. However, applications of these algorithms in discrete element codes need modifications to meet the needs of particular discrete element body representations and the kinematic resolution.

For the detection of potential contact between a large number of discrete elements, a spatial search algorithm based on space-cell subdivision and incorporating a tree data storage structure possesses significant computational advantages. For instance, the augmented spatial digital tree (Feng *et al* 2002) is a spatial binary tree based contact detection algorithm. It uses the lower corner vertex to represent a rectangle in a binary spatial tree, with the upper corner vertex serving as the augmented information. The algorithm is insensitive to the size distributions of the discrete objects. Numerical experiments in (Feng *et al* 2002) indicate that this search algorithm can reduce the CPU requirement of a contact detection from an originally demanding level down to a more acceptable proportion of the computing time.

Another type of the contact detection algorithms is the so-called cell based search (Munjiza *et al* 1998, Perkins *et al* 1995). The main procedures in these algorithms involve: (1) dividing the domain that the discrete objects occupy into regular grid cells; (2) mapping each discrete object to one of the grid cells; and (3) for each discrete object in a cell, checking for possible contacts with other objects in the same cell and in the neighbouring cells. Provided the number of cell columns and rows is significantly less than the number of discrete objects, it can be proved that the memory requirement for the dynamic cell search algorithm is  $O(N)$ . Also for a fixed cell size the computational time  $T_{op}$  may be expressed as

$$T_{op} = O(N + \varepsilon)$$

where  $\varepsilon$  represents the costs associated with the maintenance of various lists used in the algorithm. Numerical tests conducted in (Han *et al* 2007b) show that the dynamic cell search algorithm is even more efficient than the tree based search algorithms for large scale problems.

### 2.3 Contact resolution

The identified pairs with potential contact are then kinematically resolved based on their actual shapes. The contact forces are evaluated according to certain constitutive relationship or appropriate physically based interaction laws. In general, the interaction laws describe the relationship between the overlap and the corresponding repulsive force of a contact pair. For rigid discrete elements, the interaction laws may be developed on the basis of the physical phenomena involved. The Hertz normal contact model that governs elastic contact of two spheres (assumed rigid in discrete element modelling) in the normal direction is such an example, in which the normal contact force,  $F_n$ , and the contact overlap,  $\delta$ , has the following relation

$$F_n = \frac{4E^* \sqrt{R^*}}{3} \delta^{3/2} \quad (1)$$

where

$$\frac{1}{E^*} = \frac{1 - \nu_1^2}{E_1} + \frac{1 - \nu_2^2}{E_2}$$

$$\frac{1}{R^*} = \frac{1}{R_1} + \frac{1}{R_2}$$

with  $R_1$  and  $R_2$  being the radii;  $E_1, E_2$ , and  $\nu_1, \nu_2$  are the elastic properties (Young's modulus and Poisson's ratio) of the two spheres.

For 'wet' particles the interaction laws may include the effects of a liquid bridge. In other cases, adhesion may be considered.

Energy dissipation due to plastic deformation, heat loss and material damping *etc* during contact is taken into account by adding a viscous damping term in the governing equation.

Friction is one of the fundamental physical phenomena involved in particulate systems. Although the search for a quantitative understanding of the features of friction has been in progress for several centuries, a universally accepted friction model has not yet been achieved. One difficulty is associated with the nature of the friction force near zero relative velocity, where a strong nonlinear behaviour is exhibited. The classic Coulomb friction law is usually employed in engineering applications for its simplicity. The discontinuous nature of the friction force in this model, however, imposes some numerical difficulties when the relative sliding velocity reverses its direction and/or during the transition from sliding (sticking) to sticking (sliding). The difficulties are usually circumvented by artificially introducing a 'transition zone'—which smears the discontinuity in the numerical computation.

Nevertheless, the suitability of any friction model should be carefully examined and the associated numerical issues fully investigated in order to correctly capture the physical phenomena involved.

A comprehensive study of the contact interaction laws can be found in (Han *et al* 2000a, Han *et al* 2000b).

#### 2.4 Governing equations and time stepping

The motion of the discrete objects is governed by Newton's second law of motion as

$$\begin{cases} \mathbf{M}\ddot{\mathbf{u}} + \mathbf{C}_d\dot{\mathbf{u}} = \mathbf{F}_c \\ J\ddot{\theta} = \mathbf{T}_c \end{cases} \quad (2)$$

where  $\mathbf{M}$  and  $\mathbf{C}_d$  are respectively the mass and damping matrices of the system,  $\mathbf{u}$ ,  $\dot{\mathbf{u}}$  and  $\ddot{\mathbf{u}}$  are respectively the displacement, velocity and acceleration vectors,  $J$  is the moment of inertia,  $\ddot{\theta}$  the angular acceleration,  $\mathbf{F}_c$  and  $\mathbf{T}_c$  denote the contact force and torque, respectively.

The configuration of the entire discrete system is evolved by employing an explicit time integration scheme. With this scheme, no global stiffness matrix needs to be formed and inverted, which makes the operations at each time step far less computationally intensive. However, any explicit time integration scheme is only conditionally stable. For a linear system the critical time step can be evaluated as (Belytschko *et al* 2000)

$$\Delta t_{cr} = \frac{2}{\omega_{max}} \quad (3)$$

where  $\omega_{max}$  is the maximum eigenvalue of the system. However, the above result may not be valid since a contact system is generally nonlinear, as is demonstrated in (Feng 2005). To ensure a stable and reasonably accurate solution, the critical time step chosen should be much smaller than the value given in Eq.(3).

### 3 Fluid-Particle Interactions

As pointed out earlier, the interaction between fluid and particles is solved by a coupled technique: using the Lattice Boltzmann Method to simulate the fluid field, and the Discrete Element Method to model particle dynamics. The hydrodynamic interactions between fluid and particles are realised through an immersed boundary condition. The solution procedures are outlined as follows.

### 3.1 The Lattice Boltzmann Method

In the Lattice Boltzmann Method, the problem domain is divided into regular lattice nodes. The fluid is modelled as a group of fluid particles that are allowed to move between lattice nodes or stay at rest. During each discrete time step of the simulation, fluid particles move to the nearest lattice node along their directions of motion, where they 'collide' with other fluid particles that arrive at the same node. By tracking the evolution of fluid particle distributions, the macroscopic variables, such as velocity and pressure, of the fluid field can be conveniently calculated from its first two moments.

The lattice Boltzmann equation with a single relaxation time for the collision operator is expressed as

$$f_i(\mathbf{x} + \mathbf{e}_i \Delta t, t + \Delta t) - f_i(\mathbf{x}, t) = -\frac{1}{\tau} [f_i(\mathbf{x}, t) - f_i^{eq}(\mathbf{x}, t)] \quad (4)$$

where  $f_i$  is the density distribution function of the fluid particles with discrete velocity  $\mathbf{e}_i$  along the  $i$ -th direction;  $f_i^{eq}$  is the equilibrium distribution function; and  $\tau$  is the relaxation time which controls the rate of approach to equilibrium. The left-hand side of Eq.(4) denotes a streaming process for fluid particles while the right-hand side models collisions through relaxation.

In the widely used D2Q9 model (Qian *et al* 1992), the fluid particles at each node move to their eight immediate neighbouring nodes with discrete velocities  $\mathbf{e}_i, (i = 1, \dots, 8)$ . The equilibrium distribution functions  $f_i^{eq}$  depend only on the fluid density,  $\rho$ , and velocity,  $\mathbf{v}$ , which are defined in D2Q9 model as

$$\begin{cases} f_0^{eq} = \rho \left( 1 - \frac{3}{2c^2} \mathbf{v} \cdot \mathbf{v} \right) \\ f_i^{eq} = w_i \rho \left( 1 + \frac{3}{c^2} \mathbf{e}_i \cdot \mathbf{v} + \frac{9}{2c^4} (\mathbf{e}_i \cdot \mathbf{v})^2 - \frac{3}{2c^2} \mathbf{v} \cdot \mathbf{v} \right) \end{cases} \quad (i = 1, \dots, 8) \quad (5)$$

in which  $c = \Delta x / \Delta t$  is the lattice speed with  $\Delta x$  and  $\Delta t$  being the lattice spacing and time step, respectively;  $w_i$  is the weighting factor with  $w_0 = \frac{4}{9}$ ,  $w_{1-4} = \frac{1}{9}$ ,  $w_{5-8} = \frac{1}{36}$ .

The macroscopic fluid variables, density  $\rho$  and velocity  $\mathbf{v}$ , can be recovered from the distribution functions as

$$\rho = \sum_{i=0}^8 f_i \quad \rho \mathbf{v} = \sum_{i=1}^8 f_i \mathbf{e}_i \quad (6)$$

The fluid pressure field  $p$  is determined by the following equation of state

$$p = c_s^2 \rho \quad (7)$$

where  $c_s$  is termed the fluid speed of sound and is related to the lattice speed  $c$  by

$$c_s = c/\sqrt{3} \quad (8)$$

The kinematic viscosity,  $\nu$ , of the fluid is implicitly determined by the model parameters,  $\Delta x$ ,  $\Delta t$  and  $\tau$  as

$$\nu = \frac{1}{3} \left( \tau - \frac{1}{2} \right) \frac{\Delta x^2}{\Delta t} = \frac{1}{3} \left( \tau - \frac{1}{2} \right) c \Delta x \quad (9)$$

which indicates that the selection of these three parameters should be correlated to achieve a correct fluid viscosity.

It can be proved that the lattice Boltzmann equation (4) recovers the incompressible Navier-Stokes equations to the second order in both space and time (Chen *et al* 1998), which is the theoretical foundation for the success of the Lattice Boltzmann Method for modelling general fluid flow problems. However, since it is obtained by the linearised expansion of the original kinetic theory based Boltzmann equation, Eq. (4) is only valid for small velocities, or small 'computational' Mach number defined by

$$M_a = \frac{v_{\max}}{c} \quad (10)$$

where  $v_{\max}$  is the maximum simulated velocity in the flow.

Generally smaller Mach number implies more accurate solution. It is therefore required that

$$M_a \ll 1 \quad (11)$$

i.e., the lattice speed  $c$  should be sufficiently larger than the maximum fluid velocity to ensure a reasonably accurate solution.

### 3.2 Incorporating turbulence model in the lattice Boltzmann equation

As many fluid-particle interaction problems are turbulent in nature, a turbulence model should be incorporated into the lattice Boltzmann equation (4).

The Large Eddy Simulation, amongst various turbulence models, solves large scale turbulent eddies directly but the smaller scale eddies using a sub-grid model. The separation of these scales is achieved through the filtering of the Navier-Stokes equations, from which the solutions to the resolved scales are directly obtained. Unresolved scales can be modelled by, for instance, the Smagorinsky sub-grid model (Smagorinsky 1963) that assumes that the Reynolds stress tensor is dependent only on the local strain rate.

Yu *et al* proposed to incorporate the Large Eddy Simulation in the lattice Boltzmann equation by including the eddy viscosity as

$$\tilde{f}_i(\mathbf{x} + \mathbf{e}_i \Delta t, t + \Delta t) = \tilde{f}_i(\mathbf{x}, t) - \frac{1}{\tau_*} [\tilde{f}_i(\mathbf{x}, t) - \tilde{f}_i^{eq}(\mathbf{x}, t)] \quad (12)$$

where  $\tilde{f}_i$  and  $\tilde{f}_i^{eq}$  denote the distribution function and the equilibrium distribution function at the resolved scale, respectively. The effect of the unresolved scale motion is modelled through an effective collision relaxation time scale  $\tau_t$ . Thus in Eq.(12) the total relaxation time equals

$$\tau_* = \tau + \tau_t$$

where  $\tau$  and  $\tau_t$  are respectively the relaxation times corresponding to the true fluid viscosity  $\nu$  and the turbulence viscosity  $\nu_*$  defined by a sub-grid turbulence model. Accordingly,  $\nu_*$  is given by

$$\nu_* = \nu + \nu_t = \frac{1}{3}(\tau_* - \frac{1}{2})c^2\Delta t = \frac{1}{3}(\tau + \tau_t - \frac{1}{2})c^2\Delta t$$

$$\nu_t = \frac{1}{3}\tau_t c^2\Delta t$$

With the Smagorinsky model, the turbulence viscosity  $\nu_t$  is explicitly calculated from the filtered strain rate tensor  $\tilde{S}_{ij} = (\partial_j \tilde{u}_i + \partial_i \tilde{u}_j)/2$  and a filter length scale (which is equal to the lattice spacing  $\Delta x$ ) as

$$\nu_t = (S_c \Delta x)^2 \hat{S} \quad (13)$$

where  $S_c$  is the Smagorinsky constant; and  $\hat{S}$  the characteristic value of the filtered strain rate tensor  $\tilde{S}$

$$\hat{S} = \sqrt{\sum_{i,j} \tilde{S}_{ij} \tilde{S}_{ij}}$$

An attractive feature of the model is that  $\tilde{S}$  can be obtained directly from the second-order moments,  $\tilde{Q}$ , of the non-equilibrium distribution function

$$\tilde{S} = \frac{\tilde{Q}}{2\rho S_c \tau_*} \quad (14)$$

in which  $\tilde{Q}$  can be simply computed by the filtered density functions at the lattice nodes

$$\tilde{Q}_{ij} = \sum_{k=1}^8 e_{ki} e_{kj} (\tilde{f}_k - \tilde{f}_k^{eq}) \quad (15)$$

where  $e_{ki}$  is the  $k$ -th component of the lattice velocity  $\mathbf{e}_i$ . Consequently

$$\hat{S} = \frac{\hat{Q}}{2\rho S_c \tau_*} \quad (16)$$

with  $\hat{Q}$  the filtered mean momentum flux computed from  $\tilde{Q}$

$$\hat{Q} = \sqrt{2 \sum_{i,j} \tilde{Q}_{ij} \tilde{Q}_{ij}} \quad (17)$$

### 3.3 Hydrodynamic forces for fluid-particle interactions

The modelling of the interaction between fluid and particles requires a physically correct 'no-slip' velocity condition imposed on their interface. In other words, the fluid adjacent to the particle surface should have identical velocity as that of the particle surface.

Ladd (Ladd 1994) proposes a modification to the bounce-back rule so that the movement of a solid particle can be accommodated. This approach provides a relationship of the exchange of momentum between the fluid and the solid boundary nodes. It also assumes that the fluid fills the entire volume of the solid particle, or in other words, the particle is modelled as a 'shell' filled with fluid. As a result, both solid and fluid nodes on either side of the boundary surface are treated in an identical fashion. It has been observed, however, that the computed hydrodynamic forces may suffer from severe fluctuations when the particle moves across the grid with a large velocity. This is mainly caused by the stepwise representation of the solid particle boundary and the constant changing boundary configurations.

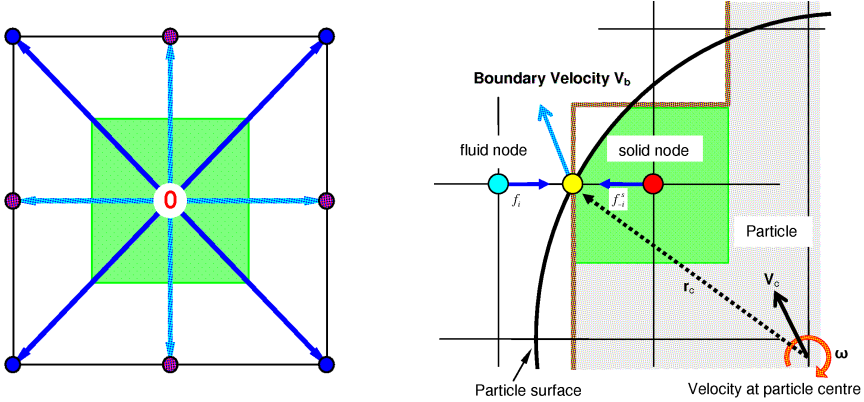
To circumvent the fluctuation of the computed hydrodynamic forces with the modified bounce-back rule, Noble and Torczynski (Noble *et al* 1998) proposed an immersed moving boundary method. In this approach, a control volume is introduced for each lattice node that is a  $\Delta x \times \Delta x$  square around the node, as illustrated by the shadow area in Fig. 1a. Meanwhile, a local fluid to solid ratio  $\gamma$  is defined, which is the volume fraction of the nodal cell covered by the particle as shown in Fig. 1b.

The lattice Boltzmann equation for those lattice nodes (fully or partially) covered by a particle is modified to enforce the 'no-slip' velocity condition as

$$f_i(\mathbf{x} + \mathbf{e}_i \Delta t, t + \Delta t) = f_i(\mathbf{x}, t) - \frac{1}{\tau} (1 - \beta) [f_i(\mathbf{x}, t) - f_i^{eq}] + \beta f_i^m \quad (18)$$

where  $\beta$  is a weighting function depending on the local fluid/solid ratio  $\gamma$ ; and  $f_i^m$  is an additional term that accounts for the bounce back of the non-equilibrium part of the distribution function, computed by the following expressions

$$\begin{cases} \beta = \frac{\gamma(\tau-0.5)}{(1-\gamma)+(\tau-0.5)} \\ f_i^m = f_{-i}(\mathbf{x}, t) - f_i(\mathbf{x}, t) + f_i^{eq}(\rho, \mathbf{v}_b) - f_{-i}^{eq}(\rho, \mathbf{v}) \end{cases} \quad (19)$$



(a) Control area of a node

(b) Nodal solid area fraction

Figure 1: Immersed boundary scheme of Noble and Torczynski

where  $-i$  denotes the opposite direction of  $i$ .

The total hydrodynamic forces and torque exerted on a particle over  $n$  particle-covered nodes are summed up as

$$\mathbf{F}_f = c \Delta x \left[ \sum_n \left( \beta_n \sum_i f_i^m \mathbf{e}_i \right) \right] \quad (20)$$

$$\mathbf{T}_f = c \Delta x \left[ \sum_n (\mathbf{x} - \mathbf{x}_c) \times \left( \beta_n \sum_i f_i^m \mathbf{e}_i \right) \right] \quad (21)$$

where  $\mathbf{x}_c$  is the coordinate of the particle center.

With this approach, the computed hydrodynamic forces are sufficiently smooth, which is also confirmed in our previous numerical tests (Feng *et al* 2007, Han *et al* 2007a).

### 3.4 Fluid and particle coupling

Fluid and particle coupling at each time step is realised by first computing the fluid solution, and then updating the particle positions through the integration of the equations of motion given by

$$\begin{cases} m\mathbf{a} + c_d\mathbf{v} = \mathbf{F}_c + \mathbf{F}_f + m\mathbf{g} \\ J\ddot{\theta} = \mathbf{T}_c + \mathbf{T}_f \end{cases} \quad (22)$$

where  $m$  and  $J$  are respectively the mass and the moment of inertia of the particle;  $\ddot{\theta}$  the angular acceleration;  $\mathbf{g}$  the gravitational acceleration if considered;  $\mathbf{F}_f$  and  $\mathbf{T}_f$

are respectively the hydrodynamic force and torque;  $\mathbf{F}_c$  and  $\mathbf{T}_c$  denote the contact force and torque from other particles and/or boundary walls;  $c_d$  is a damping coefficient and the term  $c_d \mathbf{v}$  represents a viscous force that accounts for the effect of all possible dissipation forces in the system. The static buoyancy force of the fluid is taken into account by reducing the gravitational acceleration to  $(1 - \rho/\rho_s) \mathbf{g}$ , where  $\rho_s$  is the density of a particle.

This dynamic equation governing the evolution of the system can be solved by the central difference scheme. Some important computational issues regarding the solution are briefly discussed as follows.

**(1). Subcycling time integration.** There are two time steps used in the coupled procedure,  $\Delta t$  for the fluid flow and  $\Delta t_d$  for the particles. Since  $\Delta t_d$  is generally smaller than  $\Delta t$ , it has to be reduced to  $\Delta t_s$  so that the ratio between  $\Delta t$  and  $\Delta t_s$  is an integer  $n_s$ :

$$\Delta t_s = \frac{\Delta t}{n_s} \quad (n_s = \lceil \Delta t / \Delta t_d \rceil + 1) \quad (23)$$

where  $\lceil \cdot \rceil$  denotes an integer round-off operator. This basically gives rise to a so-called subcycling time integration for the discrete element part; in one step of the fluid computation,  $n_s$  sub-steps of integration are performed for Eq. (22) using the time step  $\Delta t_s$ ; whilst the hydrodynamic forces  $\mathbf{F}_f$  and  $\mathbf{T}_f$  are kept unchanged during the subcycling.

**(2). The dynamic equation in the lattice coordinate system.** Since the lattice Boltzmann equation is implemented in the lattice coordinate system in this work, the dynamic equation Eq. (22) should be implemented in the same way. It can be derived that in the lattice coordinate system Eq. (22) takes the form of

$$\bar{m} \bar{\mathbf{a}} + \bar{c}_d \bar{\mathbf{v}} = \bar{\mathbf{F}}_c + \bar{\mathbf{F}}_f + \bar{m} \bar{\mathbf{g}} \quad (24)$$

where

$$\begin{cases} \bar{m} = m/\rho_s \Delta x^2 & \bar{\mathbf{v}} = \mathbf{v}/c \\ \bar{\mathbf{a}} = \mathbf{a} \Delta t/c; & \bar{\mathbf{g}} = \mathbf{g} \Delta t/c \\ \bar{c}_d = c \Delta x c_d; & \bar{\mathbf{F}}_t = \mathbf{F}_t / (\rho_0 c^2 \Delta x) \end{cases}$$

### 3.5 Numerical illustration

To assess the applicability of the combined lattice Boltzmann and discrete element approach proposed in this section, a vacuum dredging system for mineral recovery is simulated. This recovery operation employs a suction process to extract rock fragments. The system consists of a rigid pipe connected to a slurry transport system, which is typically powered by a gravel pump. The gravel is transported to the pipe entrance via hydraulic entrainment.

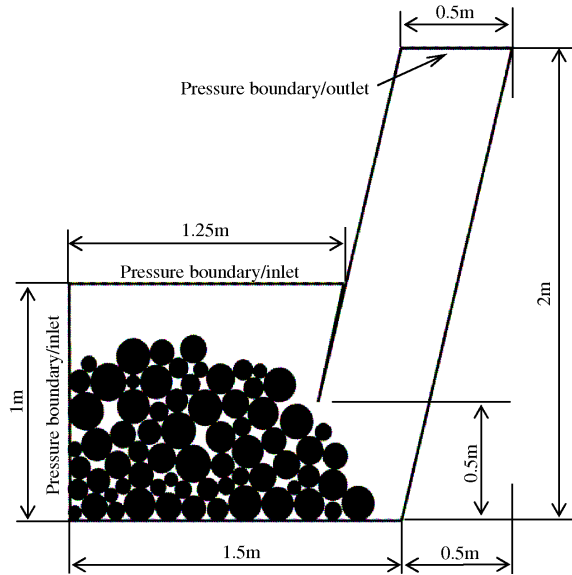


Figure 2: Problem description

The problem is illustrated in Fig. 2, where the two inclined lines represent the pipe boundaries. The fluid domain is divided into a  $800 \times 800$  square lattice with spacing  $\Delta x = 2.5mm$ . Though the fluid domain should be rectangular in the Lattice Boltzmann Method, a polygonal fluid domain is taken as the actual computational domain to reduce the computational cost since both left-top and right-bottom sub-domains can be excluded from the simulation. To accommodate this irregularity, the actual domain profile is identified first, and the lattice Boltzmann equation (4) is applied only to the nodes within the profile. This is a generic approach which can be extended to any problem with an irregular exterior domain boundary. The fluid is water with density  $\rho = 1000kg/m^3$  and kinematic viscosity  $\nu = 10^{-6}m^2/s$ . A constant pressure boundary condition with  $\rho_{in} = \rho$  is imposed to the two (inlet) boundaries as shown in the figure. A smaller pressure with  $\rho_{out} = 0.97\rho$  is applied to the outlet of the pipe. The remaining boundaries are assumed stationary walls.

A total of 70 circular particles with different sizes uniformly distributed in the range of 30 – 80mm are randomly positioned at the bottom of the domain. Full gravity ( $g = 9.81m/s^2$ ) is applied. The Hertzian contact model is used to model the contact between the particles and between particles and walls. The following parameters are chosen: particle density  $\rho_s = 5000kg/m^3$ ; contact damping ratio  $\xi = 0.5$  and time step factor  $\lambda = 0.1$ , which gives a time step of  $\Delta t_D = 3.37 \times 10^{-5}$  for the discrete element simulation of the particles.

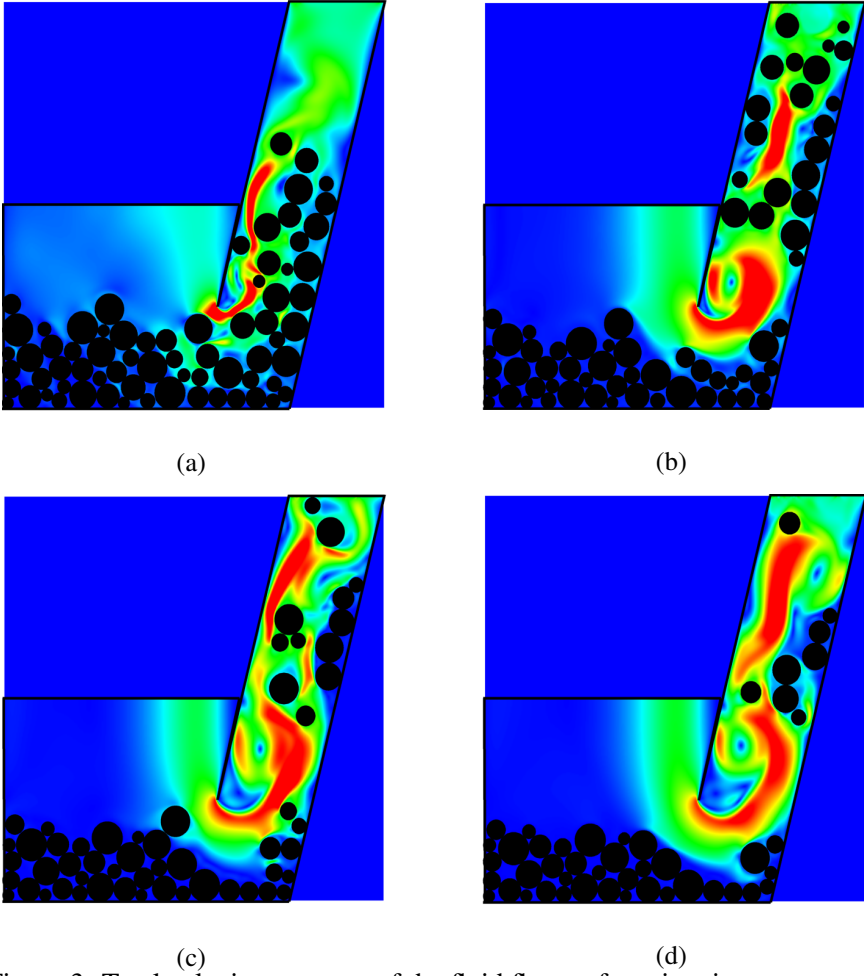


Figure 3: Total velocity contours of the fluid flow at four time instants

The Smagorinsky turbulence model with the Smagorinsky constant  $S_c = 0.1$  is adopted. A complete simulation is achieved with  $\tau = 0.501$ . This gives a time step  $\Delta t = 4.17 \times 10^{-5} s$  and thus the corresponding lattice speed  $c = 60 m/s$ . The subcycle number  $n_s$  is computed as  $n_s = 2$ . The simulated maximum fluid velocity is approximately  $v_{max} = 5.6 m/s$  at the pipe outlet (with the characteristic length being the pipe diameter,  $L = D = 0.5 m$ ). The maximum Mach number and Reynolds number are therefore estimated as

$$M_a = \frac{v_{max}}{c} = 0.0933; \quad R_e = \frac{v_{max} * L}{\nu} = 2.8 \times 10^6$$

The Mach number indicates that the results obtained are reasonably accurate. The flow field in terms of the total velocity contour and the evolution of the particles at four time instants are depicted in Figs.3(a)-(d), from which the complex fluid flow patterns due to fluid-particle interactions, particle/particle and particle/wall collisions are clearly observed. The general pattern and behaviour of the entire system appears realistic.

## 4 Thermal-Particle Interactions

### 4.1 Convective heat transfer

If an additional field, *thermal*, exists, the Thermal Lattice Boltzmann Method is adopted to account for heat exchange between particles and between particles and the surrounding fluid. In the double-population model (He *et al* 1998), in addition to the evolution equation for fluid flow (Eq.(4)), an internal energy distribution function is also introduced to solve thermodynamics, as described by the following evolution equation,

$$\bar{g}_i(\mathbf{x} + \mathbf{e}_i \Delta t, t + \Delta t) - \bar{g}_i(\mathbf{x}, t) = -\frac{1}{\tau_g + 0.5} [\bar{g}_i(\mathbf{x}, t) - g_i^{eq}(\mathbf{x}, t)] - \frac{\tau_g}{\tau_g + 0.5} f_i Z_i \quad (25)$$

where

$$\bar{f}_i = f_i + \frac{0.5}{\tau_f} (f_i - f_i^{eq}) \quad (26)$$

$$\bar{g}_i = g_i + \frac{0.5}{\tau_g} (g_i - g_i^{eq}) + \frac{\Delta t}{2} f_i Z_i \quad (27)$$

in which  $g_i$  is the internal energy distribution function with discrete velocity  $\mathbf{e}_i$  along the  $i$ -th direction;  $g_i^{eq}$  is the corresponding equilibrium distribution function;  $\tau_g$  is the internal energy relaxation time which controls the rate of change to equilibrium.

The term  $Z_i = (\mathbf{e}_i - \mathbf{v}) \cdot [\partial \mathbf{v} / \partial t + (\mathbf{e}_i \cdot \nabla) \mathbf{v}]$  represents the effect of viscous heating and can be expressed as

$$Z_i = \frac{(\mathbf{e}_i - \mathbf{v}) \cdot [\mathbf{v}(\mathbf{x} + \mathbf{e}_i \Delta t, t + \Delta t) - \mathbf{v}(\mathbf{x}, t)]}{\Delta t} \quad (28)$$

For gas flow, the lattice speed  $c$  can be defined as

$$c = \sqrt{3RT_m}$$

where  $R$  is the gas constant and  $T_m$  the average temperature.

The internal energy equilibrium distribution functions  $g_i^{eq}$  are defined in the D2Q9 model as

$$\begin{cases} g_0^{eq} = w_0 \rho \varepsilon \left[ -\frac{3(\mathbf{v} \cdot \mathbf{v})}{2c^2} \right] \\ g_i^{eq} = w_i \rho \varepsilon \left[ \frac{3}{2} + \frac{3(\mathbf{e}_i \cdot \mathbf{v})}{2c^2} + \frac{9(\mathbf{e}_i \cdot \mathbf{v})^2}{2c^4} - \frac{3(\mathbf{v} \cdot \mathbf{v})}{2c^2} \right] & (i = 1, 2, 3, 4) \\ g_i^{eq} = w_i \rho \varepsilon \left[ 3 + \frac{6(\mathbf{e}_i \cdot \mathbf{v})}{c^2} + \frac{9(\mathbf{e}_i \cdot \mathbf{v})^2}{2c^4} - \frac{3(\mathbf{v} \cdot \mathbf{v})}{2c^2} \right] & (i = 5, 6, 7, 8) \end{cases} \quad (29)$$

in which  $w_i$  are the weighting factors with the same values as defined in Section 3.1; and  $\rho \varepsilon$  denotes the internal energy.

The internal energy per unit mass  $\varepsilon$  and heat flux  $q$  can be calculated from the zeroth and first order moments of the distribution functions as

$$\rho \varepsilon = \sum \bar{g}_i - \frac{\Delta t}{2} \sum f_i Z_i; \quad q = \left( \sum \mathbf{e}_i \bar{g}_i - \rho \varepsilon \mathbf{v} - \frac{\Delta t}{2} \sum \mathbf{e}_i f_i Z_i \right) \frac{\tau_g}{\tau_g + 0.5} \quad (30)$$

To evaluate the convective heat exchange between a solid particle and the surrounding fluid, the following approach is proposed in this work.

Assume that a solid particle is mapped onto the lattice by a set of lattice nodes. The nodes on the boundary of the solid region are termed boundary nodes. If  $i$  is a link (or direction) between a boundary node and a fluid node, the convective heat exchange between the solid particle and the surrounding fluid can be evaluated as

$$q = \sum_i \left[ g_{-i}(\mathbf{x}, t) - g_i(\mathbf{x}, t_+) \right] \quad (31)$$

where  $g_i(\mathbf{x}, t_+)$  denotes the post collision distribution at the boundary node  $\mathbf{x}$ , and  $-i$  is the opposite direction of  $i$ .

Our numerical tests show that the Thermal Lattice Boltzmann Method can model natural or forced convection in particulate systems well, but is not efficient to simulate heat conduction between particles, particularly for systems comprising a large number of particles. For this reason, a novel numerical approach, termed the Discrete Thermal Element Method (Feng *et al* 2008), is proposed, which is outlined in the following.

#### 4.2 Conductive heat transfer in particles

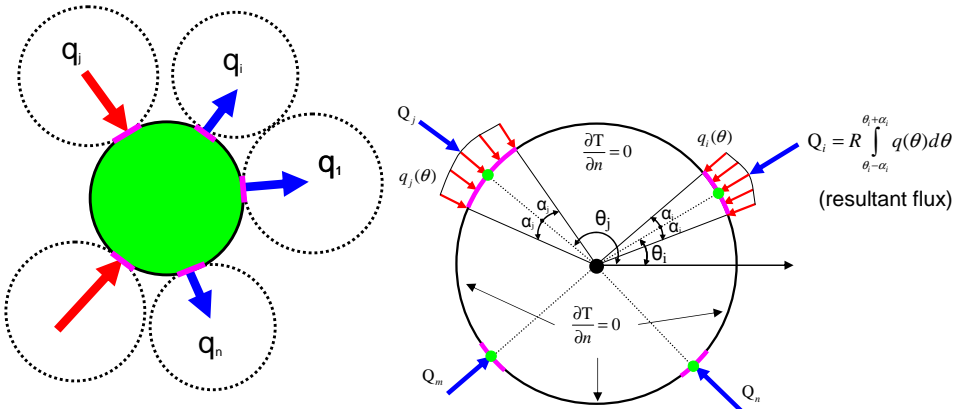
Consider a circular particle of radius  $R$  in a particle assembly that is in contact with  $n$  neighboring particles, as shown in Fig. 4a, in which heat is conducted only through the  $n$  contact zones on the boundary of the particle, and the rest of the particle boundary is fully insulated. A polar coordinate system  $(r, \theta)$  is established

with the origin set at the centre of the particle. Each contact zone (assumed to be an arc) can be described by the position angle  $\theta$  and the contact angle  $\alpha$  in Fig. 4b. In general situations the position angles are well spaced along the boundary and the contact angles  $\alpha_i$  are small. The position and contact angles of the  $n$  contact zones constitute the local element (contact) configuration of the particle. Furthermore, if the heat flux along the  $i$ -th contact zone is described by a (local) continuous function  $q_i(\theta)$ , then the heat flux on the boundary of the particle can be represented as

$$q(\theta) = \begin{cases} q_i(\theta - \theta_i) & \theta_i - \alpha_i \leq \theta \leq \theta_i + \alpha_i \quad (i = 1, \dots, n) \\ 0 & \text{otherwise} \end{cases} \quad (32)$$

The heat flux equilibrium in the particle requires

$$\int_0^{2\pi} q(\theta) d\theta = 0 \quad (33)$$



(a) A circular particle in an assembly

(b) Thermal particle representation

Figure 4: Heat conduction in a simple particle system

The temperature distribution  $T(r, \theta)$  within the particle domain  $\Omega = \{(r, \theta) : 0 \leq r \leq R; 0 \leq \theta \leq 2\pi\}$  is governed by the Laplace equation as:

$$\begin{cases} \kappa \Delta T = 0 & \text{in } \Omega \\ \kappa \frac{\partial T}{\partial n} = q(\theta) & \text{on } \partial \Omega \end{cases} \quad (34)$$

where  $\kappa$  is the thermal conductivity;  $\partial\Omega$  denotes the boundary (circumference) of the particle; and  $\frac{\partial T}{\partial n}$  is the temperature gradient along the normal direction to the boundary. Then the temperature at any point  $(r, \theta) \in \Omega$  can be expressed as

$$T(r, \theta) = -\frac{R}{2\pi\kappa} \int_0^{2\pi} q(\phi) \ln \left[ 1 - 2\frac{r}{R} \cos(\theta - \phi) + \left(\frac{r}{R}\right)^2 \right] d\phi + T_o \quad (r, \theta) \in \Omega \quad (35)$$

where  $T_o$  is the temperature at the centre, i.e.  $T_o = T(0, 0)$ .

The solutions (35) are in integral form which provide an explicit formulation to evaluate the temperature distribution over the particle when the input heat flux along the boundary is given.

The temperature distribution along the  $i$ -th contact arc is given by

$$T_c^i(\theta) = -\frac{R}{\pi\kappa} \sum_{j=1}^n \int_{-\alpha_j}^{\alpha_j} q_j(\phi) \ln \left| \sin \frac{\theta - \phi - \theta_j}{2} \right| d\phi + T_o \quad (\theta_i - \alpha_i \leq \theta \leq \theta_i + \alpha_i) \quad (36)$$

Define  $T_i$  and  $Q_i$  respectively as the average temperature and the resultant flux on the  $i$ -th arc and further assume that  $q_i(\theta)$  is constant. Then  $T_i$  can be obtained as

$$T_i = \sum_{j=1}^n \left[ -\frac{Q_j}{4\pi\kappa\alpha_i\alpha_j} \int_{-\alpha_i}^{\alpha_i} \int_{-\alpha_j}^{\alpha_j} \ln \left| \sin \frac{\Delta\theta_{ij} + \theta - \phi}{2} \right| d\phi d\theta \right] + T_o \quad (37)$$

or

$$T_i = \sum_{j=1}^n h_{ij} Q_j + T_o \quad (i = 1, \dots, n) \quad (38)$$

where

$$h_{ij} = h_{ji} = -\frac{1}{4\pi\kappa\alpha_i\alpha_j} \int_{-\alpha_i}^{\alpha_i} \int_{-\alpha_j}^{\alpha_j} \ln \left| \sin \frac{\Delta\theta_{ij} + \theta - \phi}{2} \right| d\phi d\theta > 0 \quad (39)$$

With the introduction of the particle (element) temperature vector  $\mathbf{T}_e = \{T_1, \dots, T_n\}^T$ , the heat flux vector  $\mathbf{Q}_e = \{Q_1, \dots, Q_n\}^T$ , the particle (element) thermal resistance matrix  $\mathbf{H}_e = \{h_{ij}\}_{n \times n}$ , and  $\mathbf{e} = \{1, \dots, 1\}^T$ , Eq. (38) can be expressed in matrix form as

$$\mathbf{T}_e - \mathbf{e}T_o = \mathbf{H}_e\mathbf{Q}_e \quad (40)$$

This is the heat conduction equation of the particle in terms of thermal resistance: the temperatures at the  $n$  contact zones, relative to the average temperature  $T_0$ , can be obtained when the fluxes  $\mathbf{Q}_e$  are known. The inverse form of Eq. (40) reads

$$\widehat{\mathbf{K}}_e(\mathbf{T}_e - \mathbf{e}T_0) = \mathbf{Q}_e \quad (\widehat{\mathbf{K}}_e = \mathbf{H}_e^{-1}) \quad (41)$$

In both Eqs.(40) and (41), the average temperature  $T_0$  can be treated as a unknown internal variable which can be obtained by a linear combination of the discrete boundary temperature  $\mathbf{T}_e$  as

$$T_0 = \mathbf{g}_e^T \mathbf{T}_e / \kappa_e \quad (\mathbf{g}_e = \widehat{\mathbf{K}}_e \mathbf{e}, \quad \kappa_e = \mathbf{e}^T \widehat{\mathbf{K}}_e \mathbf{e}) \quad (42)$$

Eliminating  $T_0$  from Eq. (41) based on relation (42), we have

$$\mathbf{K}_e \mathbf{T}_e = \mathbf{Q}_e \quad (43)$$

where

$$\mathbf{K}_e = \widehat{\mathbf{K}}_e - \mathbf{g}_e \mathbf{g}_e^T / \kappa_e$$

is the heat conductivity matrix of the particle.

Eq. (43) is the heat conduction equation in discrete form for the particle, which is termed the *discrete thermal element*. It has an identical form as a thermal finite element. Thus the subsequent procedure to model heat conduction in the particle system can follow the same procedure as those of the conventional finite element analysis.

This discrete thermal element approach provides a simple and accurate heat conduction model for a circular particle in which the temperature field within the particle is fully resolved, which is a distinct advantage over the existing isothermal models.

In the discrete thermal element, the temperature distribution in a particle is a linear superposition of the contributions from all the heat fluxes at the thermal contact zones. Specifically, the temperature at the  $i$ -th zone,  $T_i$ , depends not only on the flux  $Q_i$  of the zone, but also on other fluxes  $Q_j$ . This coupling effect is accounted for by the off-diagonal terms,  $h_{ij}$ , in the thermal resistance matrix  $\mathbf{H}_e$ . The numerical evaluation conducted in (Feng *et al* 2008) shows that a typical value of  $h_{ij}$  is about 10 times smaller than that of the diagonal terms  $h_{ii}$ , which implies that the coupling effect between different zones is fairly weak. This observation promotes the development of a simplified version of the discrete thermal element formulation, termed the pipe-network model.

In the pipe-network model, the off-diagonal terms in the thermal resistance matrix  $\mathbf{H}_e$  is neglected such that

$$\bar{\mathbf{H}}_e = \text{diag}\{h_{ii}\}$$

Then the original equations (40) are fully decoupled:

$$T_i - T_o = h_{ii} Q_i \quad (i = 1, \dots, n) \quad (44)$$

The resulting decoupled thermal equations can be conceptually represented by a simple star-shaped 'pipe' network model, as shown in Fig. 5. For an individual pipe  $i$ , the corresponding thermal resistance  $R_i$  and conductivity  $k_i$  are given by

$$R_i = h_{ii}; \quad k_i = 1/R_i = 1/h_{ii} \quad (45)$$

and Eq. (44) can be rewritten as

$$k_i(T_i - T_o) = Q_i \quad (i = 1, \dots, n) \quad (46)$$

In this model,  $T_o$  plays a central role. If no external heat source is applied, the net flux at the centre must equal zero due to the heat flux equilibrium requirement  $\sum Q_i = 0$ . Then Eq. (42) can be further simplified as

$$T_o = \sum_{i=1}^n (k_i T_i) / \sum_{i=1}^n k_i \quad (47)$$

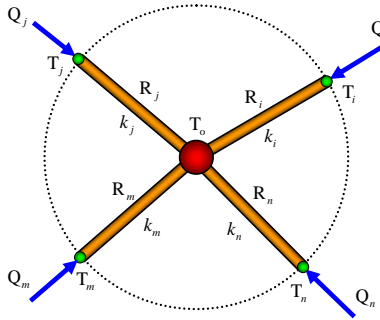


Figure 5: Pipe-network model

With the pipe-network model, the transient analysis can be readily performed.

The governing equation for the transient heat conduct analysis of a solid is expressed as

$$\rho c_p \dot{T} + \kappa \Delta T = 0 \quad (48)$$

where  $\rho$  and  $c_p$  are the density and the specific heat capacity of the solid, respectively;  $\dot{T} = \partial T / \partial t$  with  $t$  being the time.

Within the pipe-network framework, the corresponding discrete version of the transient equation (48) for the  $i$ -th particle can be expressed as

$$C_i \dot{T}_i^o + \sum_{j=1}^n Q_{ij} = 0 \quad (49)$$

where  $Q_{ij}$  are the internal heat fluxes associated with the particle defined by

$$Q_{ij} = k_{ij}(T_j^o - T_i^o) \quad (50)$$

and  $C_i$  is the total heat capacity of the particle, given by

$$C_i = \pi \rho c_p R_i^2$$

The global system of equations can be assembled as

$$\mathbf{C}\mathbf{T}^o(t) + \mathbf{K}_g\mathbf{T}^o(t) = \mathbf{Q}(t) \quad (51)$$

where the global heat capacity matrix  $\mathbf{C} = \text{diag}\{C_i\}$  is a diagonal matrix,  $\mathbf{K}_g$  is the global stiffness matrix, and  $\mathbf{T}^o = \{T_1^o, \dots, T_m^o\}^T$  is the average temperature vector of the particles. The system can be solved either explicitly or implicitly.

The formulation of the pipe-network model is compatible with that of the Discrete Element Method, which makes the thermal and mechanical coupling possible.

### 4.3 Numerical illustration

The solution accuracy of the Discrete Thermal Element Method for steady-state analysis has been assessed in (Feng *et al* 2008) via a number of numerical tests. In this subsection, an example is provided to illustrate the capability of the pipe-network model for thermal transient analysis.

The simulation is performed for a particle assembly with 265 particles. The outer walls are assumed insulated (achieved by detaching the walls from the particles), and each particle in the assembly is assigned an initial temperature  $T_i^0$  with a random value between 0 and 1. The density and the specific heat capacity of the particles are assumed to be 1 and 10, respectively. A backward Euler scheme is employed to solve the global equations, with a fixed time step  $\Delta t = 0.1s$ . The equilibrium (steady-state) temperature of the system can be found as

$$T = \sum_i C_i T_i^0 / \sum_i C_i$$

Fig. 6 depicts the average particle temperature distributions at four time instants, where the temperature convergence to the steady-state is evident. The time evolution histories of the average temperatures (relative to the final steady-state temperature  $T$ ) for two particles randomly chosen from the assembly are plotted in Fig. 7, again indicating the temperatures approaching to the correct steady-state value.

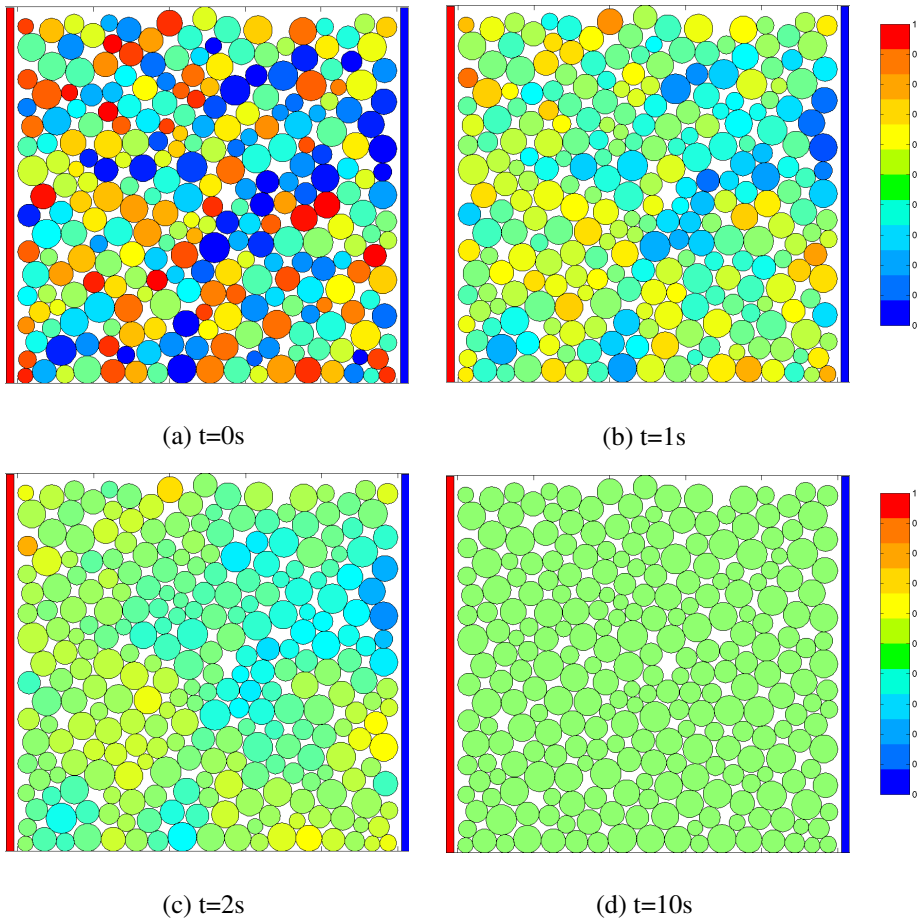


Figure 6: Average particle temperature distributions at four time instants

## 5 Fluid-Thermal-Particle Coupling

The fluid-thermal-particle interaction can be fully coupled by employing the numerical procedures described in the preceding sections: the fluid-particle interaction is modelled by the coupled Lattice Boltzmann and the Discrete Element Methods; while the fluid-thermal and particle-thermal interactions are simulated jointly by the Thermal Lattice Boltzmann Method and the Discrete Thermal Element Method, as schematically illustrated in Fig.8.

The applicability of the solution methodology is illustrated by simulating the velocity and temperature fields of a moving particle system with heat transfer. The problem considered is a randomly packed particle bed of dimensions  $0.5m \times 1.0m$ .

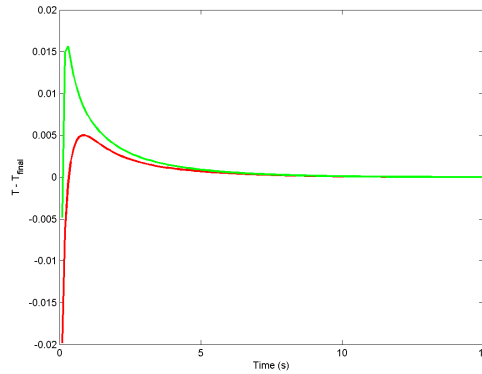


Figure 7: Temperature evolution histories of two particles

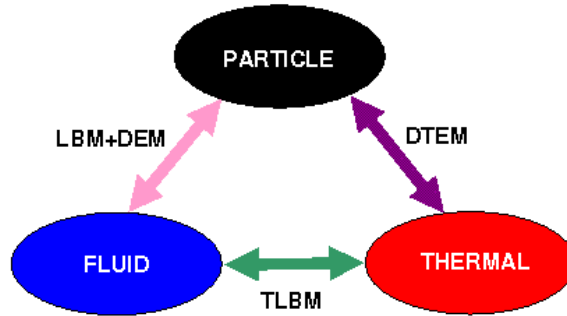


Figure 8: Fluid-thermal-particle coupling

The initial temperature of the 512 particles is set in the range of  $[20, 100]^{\circ}\text{C}$ . A hot gas ( $100^{\circ}\text{C}$ ) flow is introduced from the bottom of the bed throughout the simulation, while the other boundaries are fully insulated. Full gravity is applied.

The physical properties are chosen as: for particles, radius  $R = 1 - 2\text{mm}$ , density  $\rho_s = 2500\text{kg/m}^3$ , heat capacity  $c_s = 150\text{J/kgK}$ , thermal conductivity  $k_s = 35\text{W/mK}$ ; whereas for the fluid (gas), density  $\rho_f = 1.0\text{kg/m}^3$ , kinematic viscosity  $\nu = 10^{-5}\text{m}^2/\text{s}$ , heat capacity  $c_f = 1005\text{J/kgK}$  and thermal conductivity  $k_f = 0.024\text{W/mK}$ . The fluid domain is divided into a  $250 \times 500$  square lattice with lattice spacing  $\Delta x = 2\text{mm}$ . The initial packing of the particles is generated using the packing algorithm proposed in (Feng *et al* 2003).

Figs. 9(a)-(d) and Figs. 10(a)-(d) show snapshot images of the velocity and temperature field evolution. It can be seen that the initially motionless particles start to move upwards when the hydrodynamic forces counteract the gravitational forces

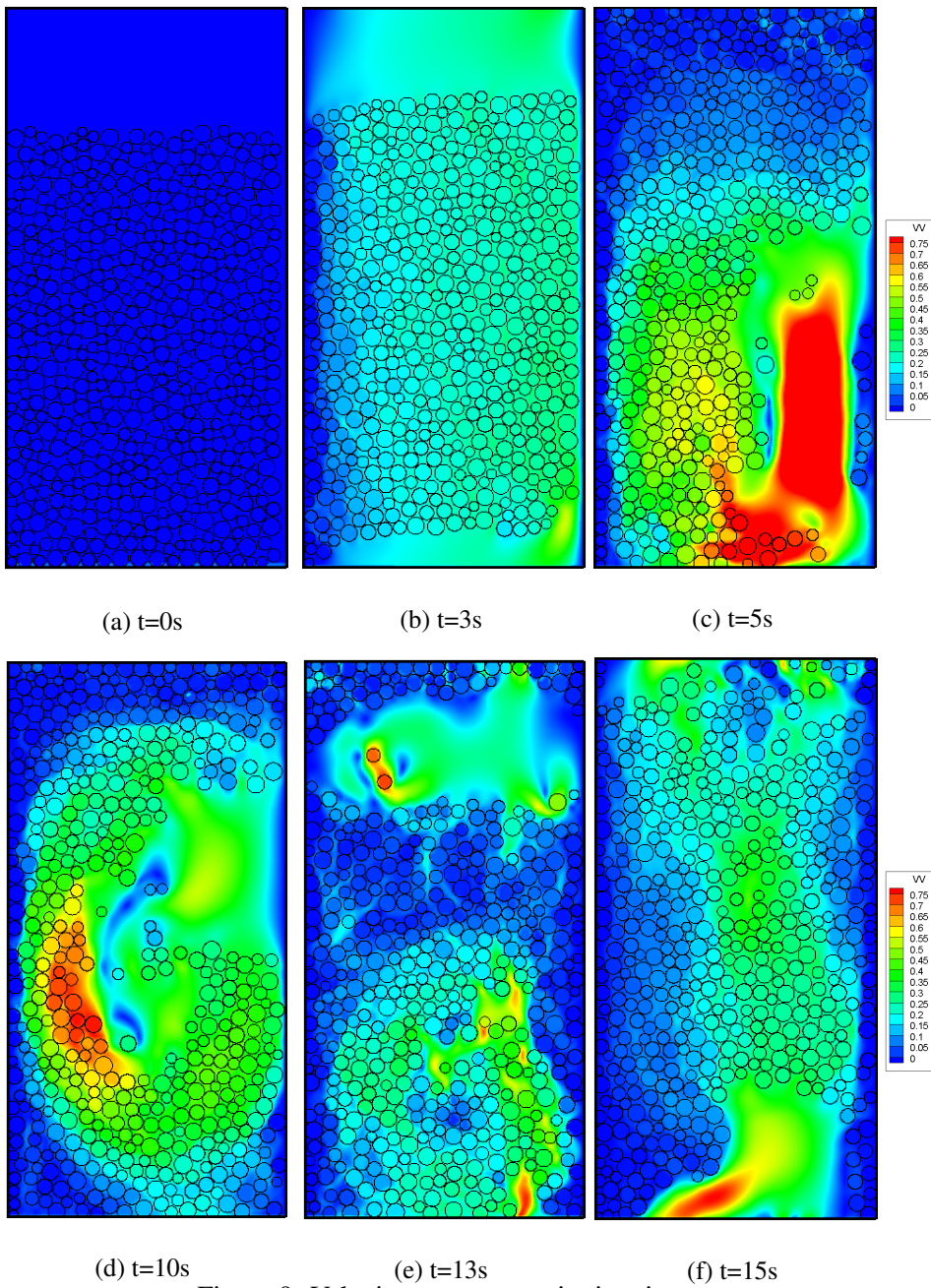
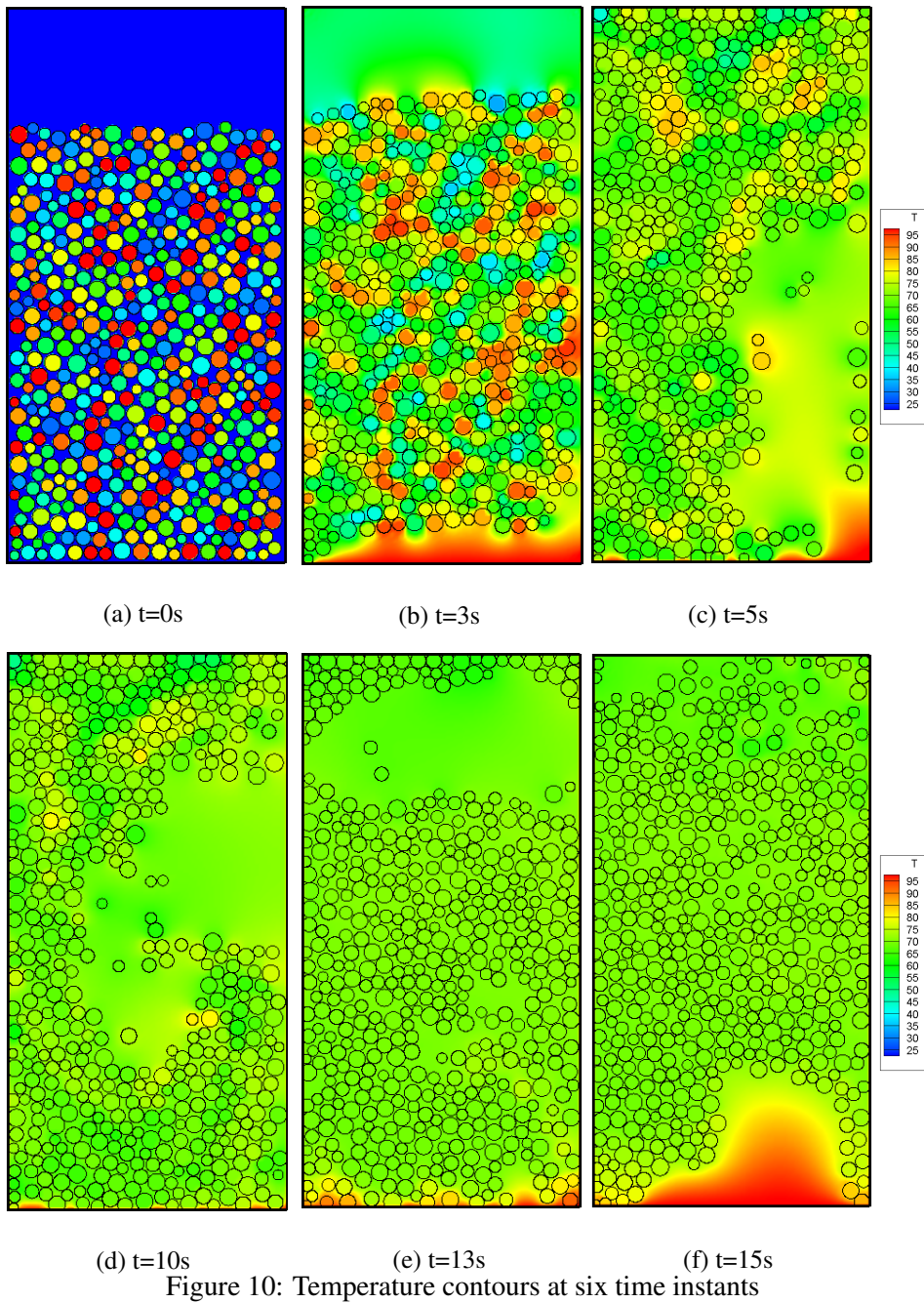


Figure 9: Velocity contours at six time instants



acting on the particles. when the velocity of the particles is low, most of the particles are in contacts and the mechanism of conductive heat transfer is significant. As the the particles moves away from each other, the convective transfer of the particles with the surrounding gas becomes dominant. Meanwhile, the particles close to the hot gas inlet (the bottom bed) get heated first and then move upwards, while the particles with lower temperatures move downwards to pick up heat. The circulation patterns of the particles and gas can be clearly seen from the pictures.

## 6 Concluding Remarks

The present work has established a computational framework for the effective coupling of fluid-thermal-particle interaction problems, in which the motion of the particles is simulated by the Discrete Element Method; the mass and velocity field of the fluid flow is modelled by the Lattice Boltzmann Method; the temperature field of the heat transfer is solved jointly by the Discrete Thermal Element Method and the Thermal Lattice Boltzmann Method. The fluid-thermal-particle interactions are realised through the hydrodynamic force terms. The applicability of the proposed approach has been illustrated via selected numerical examples.

## References

- Aidun, C. K.; Lu, Y.; Ding, E.-G.**(1998): Direct analysis of particulate suspensions with inertia using the discrete Boltzmann equation. *Journal of Fluid Mechanics*, vol.373, pp.287-311.
- Belytschko, Ted; Liu, Wing Kam; Moran, Brian**(2000): *Nonlinear finite elements for continua and structures*. John Wiley & Sons Ltd.
- Chen, S.; Doolen, G.**(1998): Lattice Boltzmann method for fluid flows. *Annual Review of Fluid Mechanics*, vol.30, pp.329-364.
- Cook, B. K.; Noble, D. R.; Williams, J.R.** (2004): A direct simulation method for particle-fluid systems. *International Journal for Engineering Computations*, vol.21, no.2-4, pp.151-168.
- Feng, Z.G.; Michaelides, E. E.**(2004): The immersed boundary-lattice Boltzmann method for solving fluid particles interaction problems. *Journal of Computational Physics*, vol.195, pp.602-628.
- Feng, Y. T.; Owen, D. R. J.**(2002): An augmented spatial digital tree algorithm for contact detection in computational mechanics. *International Journal for Numerical Methods in Engineering*, vol.55, pp.159-176.

**Feng, Y. T.; Han, K.; Owen, D. R. J.**(2003): Filling domains with disks: an advancing front approach. *International Journal for Numerical Methods in Engineering*, vol.56, pp.699-713.

**Feng, Y. T.**(2005): On the central difference algorithm in discrete element modeling of impact. *International Journal for Numerical Methods in Engineering*, vol.64, pp.1959-1980.

**Feng, Y. T.; Han, K.; Owen, D. R. J.**(2007): Coupled lattice Boltzmann method and discrete element modelling of particle transport in turbulent fluid flows: computational issues. *International Journal for Numerical Methods in Engineering*, vol.72, pp.1111-1134.

**Feng, Y. T.; Han, K.; Li, C.F.; Owen, D. R. J.**(2008): Discrete thermal element modelling of heat conduction in particle systems: basic formulations. *Journal of Computational Physics*, vol.227, pp.5072-5089.

**Feng, Y. T.; Han, K.; Owen, D. R. J.**(2009) Combined three-dimensional lattice Boltzmann and discrete element methods for modelling fluid-particle interactions with experimental validation. *International Journal for Numerical Methods in Engineering*, doi: 10.1002/nme.2689.

**Han, K.; Perić, D.; Crook, A.J.L.; Owen, D.R.J.**(2000a): A combined finite/discrete element simulation of shot peening process. part I: studies on 2D interaction laws. *International Journal for Engineering Computations*, vol.17, no.5, pp.593-619.

**Han, K.; Perić, D.; Owen, D.R.J.; Yu, J.**(2000b): A combined finite/discrete element simulation of shot peening process. part II: 3D interaction laws. *International Journal for Engineering Computations*, vol.17, no.6/7, pp.684-702.

**Han, K.; Feng, Y. T.; Owen, D. R. J.**(2007a): Numerical simulations of irregular particle transport in turbulent flows using coupled LBM-DEM. *CMES: Computer Modeling in Engineering & Science*, vol.18, no.2, pp.87-100.

**Han, K.; Feng, Y. T.; Owen, D. R. J.**(2007b): Performance comparisons of tree based and cell based contact detection algorithms. *International Journal for Engineering Computations*, vol.24, no.2, pp.165-181.

**He, X.; Chen, S.; Doolen, G.R.**(1998): A novel thermal model for the lattice Boltzmann method in incompressible limit. *Journal of Computational Physics*, vol.146, pp.282-300.

**Ho C. F., Chang C., Lin K. H., Lin C. A.**(2009): Consistent boundary conditions for 2D and 3D lattice Boltzmann simulations. *CMES: Computer Modeling in Engineering & Science*, vol.47, no.2, pp.137-156.

**Ladd, A.**(1994): Numerical simulations of fluid particulate suspensions via a discretized Boltzmann equation (Parts I & II). *Journal of Fluid Mechanics*, vol.271, pp.285-339.

**Ladd, A.; Verberg, R.** (2001): Lattice-Boltzmann simulations of particle-fluid suspensions. *Journal of Statistical Physics*, vol.104, no.5/6, pp.1191-1251.

**Mishra S. K., Paik J. K., Atluri S. N.**(2009): Modeling of the inhibition-mechanism triggered by 'smartly' sensed interfacial stress corrosion and cracking. *CMES: Computer Modeling in Engineering & Science*, vol.50, no.1, pp.67-96.

**Munjiza, A.; Andrews, K.R.F.** (1998): NBS contact detection algorithm for bodies of similar size. *International Journal for Numerical Methods in Engineering*, vol.43, pp.131-149.

**Noble, D.; Torczynski, J.** (1998): A lattice Boltzmann method for partially saturated cells. *International Journal of Modern Physics C*, vol.9, pp.1189-1201.

**Perkins, E.; Williams, J.R.** (1995): A fast contact detection algorithm insensitive to object sizes. *International Journal for Engineering Computations*, vol.12, pp.185-201.

**Qi, D.; Luo, L.** (2003): Rotational and orientational behaviour of three-dimensional spheroidal particles in Couette flows. *Journal of Fluid Mechanics*, vol.477, pp.210-213.

**Qian, Y.; d'Humieres, D.; Lallemand, P.**(1992): Lattice BGK models for Navier-Stokes equation. *Europhys. Lett.*, vol.17, pp.479-484.

**Smagorinsky, J.**(1963): General circulation model of the atmosphere. *Weather Rev.*, pp.99-164.

**Williams, J.R.; O'Connor, R.**(1995): A linear complexity intersection algorithm for discrete element simulation of arbitrary geometries. *International Journal for Engineering Computations*, vol.12, pp.185-201.

**Yu, H.; Girimaji, S.; Luo, L.**(2005): DNS and LES of decaying isotropic turbulence with and without frame rotation using lattice Boltzmann method. *Journal of Computational Physics*, vol.209, pp.599-616.

